LETTER Communicated by Jaap van Pelt

A Probabilistic Framework for Region-Specific Remodeling of Dendrites in Three-Dimensional Neuronal Reconstructions

Rishikesh Narayanan
rishi@ncbs.res.in
Anusha Narayan
anusha@caltech.edu
Sumantra Chattarji
shona@ncbs.res.in
National Centre for Biological Sciences, Bangalore 560065, India

Dendritic arborization is an important determinant of single-neuron function as well as the circuitry among neurons. Dendritic trees undergo remodeling during development, aging, and many pathological conditions, with many of the morphological changes being confined to certain regions of the dendritic tree. In order to analyze the functional consequences of such region-specific dendritic remodeling, it is essential to develop techniques that can systematically manipulate three-dimensional reconstructions of neurons. Hence, in this study, we develop an algorithm that uses statistics from precise morphometric analyses to systematically remodel neuronal reconstructions. We use the distribution function of the ratio of two normal distributed random variables to specify the probabilities of remodeling along various regions of the dendritic arborization. We then use these probabilities to drive an iterative algorithm for manipulating the dendritic tree in a region-specific manner. As a test, we apply this framework to a well-characterized example of dendritic remodeling: stress-induced dendritic atrophy in hippocampal CA3 pyramidal cells. We show that our pruning algorithm is capable of eliciting atrophy that matches biological data from rodent models of chronic stress.

1 Introduction

Dendrites are the primary sites for receiving synaptic inputs from other neurons. The structure and biophysical properties of the dendritic arbor critically modulate synaptic integration. The discovery of the presence of numerous voltage-gated ion channels in dendrites has increased the importance of the role of dendritic arbor in neuronal function (Stuart, Spruston, & Häusser, 1999; Magee, Hoffman, Colbert, & Johnston, 1998; Johnston, Magee, Colbert, & Cristie, 1996; Migliore & Shepherd, 2002). Theoretical and experimental studies point to a significant role for dendritic morphology in modulating neuronal firing patterns (Mainen & Sejnowski, 1996;

Krichmar, Nasuto, Scorcioni, Washington, & Ascoli, 2002; van Ooyen, Duijnhouwer, Remme, & van Pelt, 2002), calcium dynamics (Regehr & Tank, 1994), propagation of action potentials (Vetter, Roth, & Häusser, 2001), axonal competition (van Ooyen, Willshaw, & Ramakers, 2000), and other important biophysical properties of neurons (Segev & London, 2000; Häusser & Mel, 2003).

The functional importance of dendritic morphology is also reflected in its strict regulation during development and in the adult brain (Stuart et al., 1999). During development, dendrites undergo dramatic changes in arborization in order to formulate appropriate synaptic contacts with other neurons (Cline, 2001; Wong & Ghosh, 2002). Structural plasticity in dendrites also plays a prominent role in changes elicited by aging (Duan et al., 2003; Pyapali & Turner, 1996), hibernation (Popov, Bocharova, & Bragin, 1992), Alzheimer's disease (Anderton et al., 1998; Brizzee, 1987; Geula, 1998), temporal lobe epilepsy (Bothwell et al., 2001), brain injury and lesions (Jones & Schallert, 1994; Kevyani & Schallert, 2002), syndromes related to mental retardation (Kaufmann & Moser, 2000; Ramakers, 2002), retinal degeneration (Marc, Jones, Watt, & Strettoi, 2003), and chronic stress (McEwen, 1999; Vyas, Mitra, Rao, & Chattarji, 2002).

Detailed morphometric analyses of dendritic plasticity indicate that such remodeling is often confined to specific regions of the dendrites. For instance, stress-induced dendritic atrophy in hippocampal CA3 pyramidal cells is restricted largely to the stratum radiatum, with other regions undergoing little or no atrophy (McEwen, 1999; Vyas et al., 2002). The possibility that the functional correlates of such localized structural changes also remain localized offers exciting roles for dendritic computation and signal processing. Further, such localized dendritic remodeling promises to provide interesting and important insights into neuronal function for a number of reasons (Johnston & Amaral, 1997; Migliore & Shepherd, 2002; Segev & London, 2000; Stuart et al., 1999):

- Inputs to different regions along the dendritic tree arrive from different brain areas (see Table 1).
- Inputs to different regions along the dendritic tree have different synaptic properties (see Table 1).
- Dendritic ion channels are not uniformly distributed (e.g., the A-type transient potassium channel, cation non-specific hyperpolarization-activated channel, I_h, and the calcium-dependent channels in CA1 pyramidal cells). This could leave similar magnitudes of dendritic remodeling with different effects on various neuronal conductances, depending on the region of remodeling.
- The effects of excitatory postsynaptic potentials (EPSP) originating from a remote dendritic location, on voltage changes at the soma, depend on the distance of that dendritic region from the soma.

Table 1: Region Specificity of Inputs to the Dendritic Tree of a CA3 Pyramidal Neuron.

Dendritic Region	Distance from Soma (μm)	Receives Inputs from	Receptors
Stratum oriens[c,d]	0–400	Commissural/associational, interneurons	NMDA, AMPA $GABA_A$
Stratum pyramidale[c,d]	Soma	Interneurons	$GABA_A$
Stratum lucidum[b]	0–100	Dentate gyrus, interneurons	Kainate, AMPA $GABA_A$
Stratum radiatum[c,d]	100–350	Commissural/associational, interneurons	NMDA, AMPA $GABA_A$, $GABA_B$
Stratum lacunosum moleculare[a]	350–550	Entorhinal cortex, interneurons	NMDA, AMPA $GABA_A$, $GABA_B$

Notes: Stratum oriens forms the basal side of the tree. All other strata, except for pyramidale, form the apical side.
[a]Berzhanskaya, Urban, and Barrionuevo (1998). [b]Cossart et al. (2002). [c]Johnston and Amaral (1997). [d]Traub, Jefferys, and Whittington (1999). AMPA = α-amino-3-hydroxy-5-methyl-4-isoxazole propionate. GABA = gamma aminobutyric acid. NMDA = *N*-methyl-*D*-aspartate.

- Remodeling of different dendritic regions leads to different effects on synaptic integration, which also depends critically on the distance from the cell body and on the distribution of dendritic ion channels.
- Dendrites are capable of eliciting localized changes in excitability (Frick, Magee, & Johnston, 2004) and spatial integration (Wang, Xu, Wu, Duan, & Poo, 2003) by modifying dendritic ion channels. The expression of such localized intrinsic mechanisms can be modulated by localized dendritic remodeling.

These issues highlight the need for a formalism that allows us to systematically manipulate dendritic morphology in three-dimensional reconstructions of neurons. Hence, the goal of this study is to develop an algorithm that would systematically manipulate neuronal reconstructions to match biological data on the modulation of dendritic architecture. To this end, we use experimental data from a well-established model of structural plasticity of dendrites in the hippocampus, dendritic atrophy in CA3 pyramidal neurons induced by chronic or repeated stress, to specify the extent and location of dendritic remodeling.

2 Methodological Overview

The flow diagram in Figure 1 provides an overview of the framework used to develop and implement the analysis presented here. Previous studies (Vyas et al., 2002) from our laboratory, using Sholl's analysis of Golgi-impregnated CA3b pyramidal neurons in the rat hippocampus, have demonstrated that

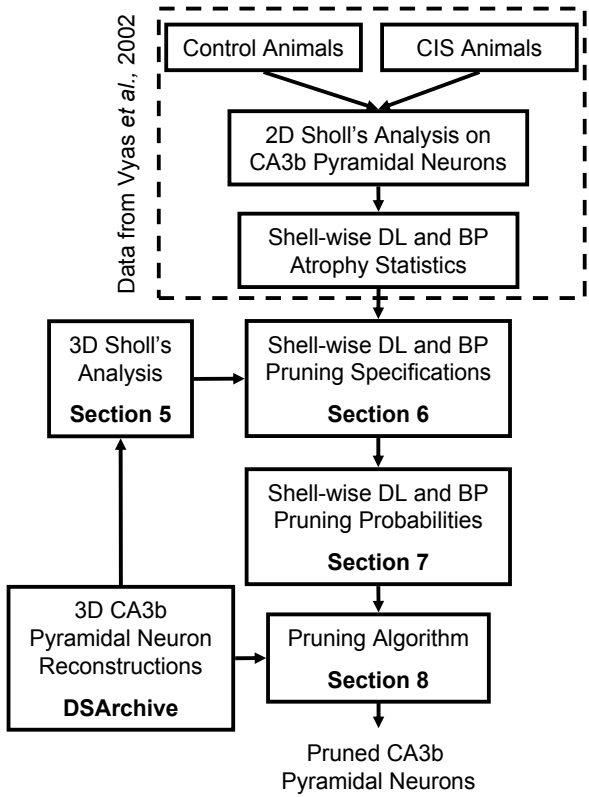

Figure 1: Overview of the methodological framework used in the study.

chronic immobilization stress (2 hours a day for 10 days) elicits specific patterns of region-specific atrophy (reduction in dendritic length, DL) and debranching (reduction in the number of branch points, BP). Thus, our experimental data (see the dotted box in Figure 1) provide region-wise statistics, for both control and stress-treated neurons, on atrophy and debranching in each concentric shell that constitutes the basic unit of two-dimensional morphometric analysis in Sholl's method (see Figure 2). These provide us with the reductions in DL and BP observed in neurons from stress-treated animals with respect to control animals.

The goal of the proposed algorithm is to enforce these experimentally observed reductions on three-dimensional (3D) neuronal reconstructions in a region-specific manner. We use digital reconstructions of CA3b pyramidal neurons from the Duke-Southampton Archive (DSArchive) as inputs to our algorithm (Cannon, Turner, Pyapali, & Wheal, 1998). There are two problems

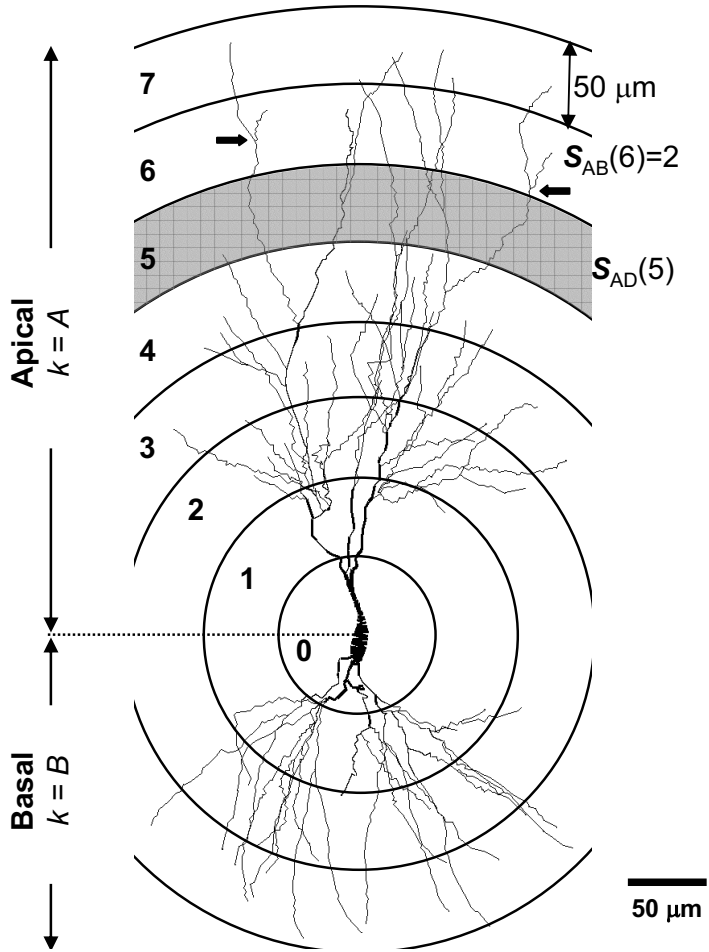

Figure 2: Illustration of Sholl's analysis and notations used. Two-dimensional projection of 3D neuronal reconstruction overlaid with concentric shells radiating out in steps of 50 μm from the center of gravity (CoG) of the soma. The number within each shell corresponds to n; the apical and basal sides of the dendritic tree are differentiated by $k = A$ and $k = B$, respectively. In this example, $\mathcal{S}_{AD}(5)$ corresponds to the dendritic length in shell number 5 along the apical side of the tree and is represented by the shaded region. $\mathcal{S}_{AB}(6)$ corresponds to the number of BPs in shell number 6 along the apical side of the tree and is equal to 2 in this case (the locations of the two BPs are indicated by arrows).

that we face in specifying the actual reductions in each concentric shell used in Sholl's analysis. First, there are considerable differences in values of DL and BP for neurons from the experimental data (two-dimensional, 2D) and DSArchive (3D). Second, each dendritic tree, for a given neuron from either database, has its own intershell variations in actual values for DL and BP. We overcome these problems by implementing an algorithm that uses the experimentally observed ratios of reduction in DL and BP as the key parameter. This ratio in turn is enforced by the algorithm on 3D neuronal reconstructions from the DSArchive.

In implementing this, in section 5, we first subject digital reconstructions of CA3b pyramidal neurons, from the DSArchive, to 3D Sholl's analysis to obtain the DLs and BPs at various distances. Next, we combine this output with experimental statistics to arrive at the pruning specifications for this neuron. We accomplish this in section 6 by arriving at DL and BP pruning specifications at various distances by sampling the ratio distribution of corresponding random variables, which are specified by experimental statistics. These specifications are then used to set the probabilities of pruning along various distances (see section 7). Finally, an iterative algorithm (see section 8) employs these probabilities to subject the 3D reconstruction to levels of dendritic atrophy and debranching that are the same as those observed in our experiments (Vyas et al., 2002). We present the results of the proposed algorithm in section 9 and discuss the implications of the study in section 10.

3 Notations

As a first step in our algorithm, we divide the dendritic tree into concentric spherical shells in order to perform Sholl's analysis on the neuron to be pruned (see section 5). Figure 2 illustrates this diagrammatically, along with providing a reference to the notations.

N_k, with $k \in \{A, B\}$, represents the number of spherical shells along apical ($k = A$) and basal ($k = B$) sides of the dendritic tree. For the neuron shown in Figure 2, $N_A = 8$ and $N_B = 4$.

$s_{kl}(n)$ and $c_{kl}(n)$ represent discrete random processes defining the BP and DL statistics in stress-treated and control animals, respectively. k, as above, denotes the class of the dendrite (apical or basal), whereas l represents whether the random process corresponds to BPs ($l = B$) or to DL ($l = D$), that is, $l \in \{B, D\}$, $n = 0, 1, \ldots, N_k - 1$. For instance, $s_{AD}(5)$ represents the random variable defining the DL in the fifth shell (250–300μm) along the apical branches in neurons from stress-treated animals (see Figure 2).

$\mu^s_{kl}(n)$ and $\mu^c_{kl}(n)$ represent the mean value of the process $s_{kl}(n)$ and $c_{kl}(n)$, respectively, and $\sigma^s_{kl}(n)$ and $\sigma^c_{kl}(n)$ represent their respective standard deviations. These are obtained directly from the DL and BP statistics of stress-treated and control animals (Vyas et al., 2002).

$\mathcal{S}_{kl}(n)$ represents the DL, obtained by subjecting the neuron to Sholl's analysis (see below), of a given 3D neuronal reconstruction with $l = D$ and $l = B$, respectively (see Figure 2 for an illustration). As above, $k \in \{A, B\}$ represents the side of the shell (apical or basal), and $n = 0, 1, \ldots, N_k - 1$ gives the shell number.

$\zeta_{kl}(n),\ n = 0, 1, \ldots, N_k - 1,\ k \in \{A, B\}$, and $l \in \{B, D\}$ are the pruning specifications, giving the amount of DL or BP to be removed from each given shell on the apical and basal sides of the neuron. Explicitly, running Sholl's analysis at the end of the pruning process should yield $\mathcal{S}_{kl}(n) - \zeta_{kl}(n)\ \forall\ k, l, n$. The probabilities for pruning DL and BP are denoted by $\rho_{kl}(n)$, $k \in \{A, B\}$, $l \in \{B, D\}$, $n = 1, \ldots, N_k - 1$, which will be derived from the pruning specifications (see section 7).

As the algorithm is an iterative one, it reduces 1 μm of dendritic length or one branching point at a time. In order to update the specifications for and probabilities of pruning at each iteration, it is necessary to keep track of the current levels of pruning, which is referred to as $\phi_{kl}(n),\ k \in \{A, B\},\ l \in \{B, D\},\ n = 0, 1, \ldots, N_k - 1$.

4 Assumptions

1. Radial isotropy is maintained in stress-induced dendritic atrophy, that is, statistics of atrophy observed in 2D morphometric data extends to the 3D case.
2. The random processes s_{kl} and c_{kl}, corresponding to stress and control statistics, respectively, are independent.
3. The random variables $s_{kl}(n),\ n = 0, 1, \ldots, N_k - 1$ are independent, as are $c_{kl}(n),\ n = 0, 1, \ldots, N_k - 1$. This assumption, given the nature of dendritic arborization, does not hold. For instance, if the number of points in shell $N_k - 2$ is zero, then the number of points in shell $N_k - 1$ has to be zero as well. However, the impact of this assumption is reduced because the pruning process takes the connectivity of the dendrites into account.
4. The random variables $s_{kl}(n)$ and $c_{kl}(n),\ n = 0, 1, \ldots, N_k - 1$ conform to a normal distribution. The normal distribution with mean μ and standard deviation σ is denoted by $N(x; \mu, \sigma)$:

$$N(x; \mu, \sigma) = \frac{1}{\sqrt{2\pi}\sigma} \exp\left(-\frac{(x-\mu)^2}{2\sigma^2}\right). \tag{4.1}$$

5 Three-Dimensional Sholl's Analysis

The first step in reproducing dendritic remodeling of model neurons similar to experimentally observed atrophy involves performing Sholl's analysis (Sholl, 1953) on digitally reconstructed neurons obtained from the

DSArchive. Neuronal morphology in the DSArchive is stored in the SWC format (Cannon et al., 1998), which consists of seven field data lines, each defining a neuronal compartment. Each SWC data line has information about the 3D coordinates of the compartment, its radius, its parent in the dendritic tree, and a type code specifying the location of the compartment (in soma, axon, basal dendrite, or apical dendrite). The 3D coordinates of the various compartments (taken from the corresponding SWC data lines) are used to reconstruct the neuron by connecting straight lines between them. Once this is done, we have access to the exact coordinates of all points along the soma and the dendritic tree. We then perform 3D Sholl's analysis on these neurons as follows (see Figure 2):

1. Calculate center of gravity (CoG) of the soma. Calculate the mean of the 3D coordinates of points associated with the soma and assign that as the center of gravity of the soma.
2. Assign shells. Construct a set of concentric spheres radiating out in steps of 50 μm from the CoG of the soma. The annular regions between these spheres form the shells, which form the basic unit of morphometric analysis using Sholl's analysis (see Figure 2). In keeping with the 3D nature of our analysis (see assumption 1, above), we employ spherical shells instead of circular shells, which are used in the traditional 2D version of Sholl's analysis (Sholl, 1953; Vyas et al., 2002).
3. Measure DL. Measure the length of dendrites within a given shell, n, by superimposing the dendritic tree on these set of concentric spheres. Assign this as $\mathcal{S}_{kD}(n)$.
4. Count BPs. Count the number of points in a given shell, n, having more than one child, and assign that as $\mathcal{S}_{kB}(n)$. In both of the above cases, the counts for the apical ($k = A$) and basal ($k = B$) sides are done separately.

6 Specification of the Pruning Schedule

The goal of the specification process is to ensure that the loss of dendritic arborization in model neurons reflects experimental data on stress-induced dendritic atrophy, where apical dendrites undergo greater atrophy than their basal counterparts and each shell along both apical and basal dendrites undergoes atrophy depending on their distance from the soma. For example, it has previously been reported (Watanabe, Gould, & McEwen, 1992; McEwen, 1999; Vyas et al., 2002) that CA3 apical dendrites in the stratum radiatum layer undergo maximal atrophy, which is in sharp contrast to little or no atrophy of basal dendrites in the stratum oriens layer.

The specification process involves setting the portion of DL to be removed from $\mathcal{S}_{kD}$ and the number of BPs to be removed from $\mathcal{S}_{kB}$, in each of the concentric shells used in Sholl's analysis. These reductions, denoted

as $\zeta_{kl}(n),\ n = 0, 1, \ldots, N_k - 1,\ k \in \{A, B\},\ l \in \{B, D\}$, are set as samples of the ratio distribution (Marsaglia, 1965) involving the DL and the BP statistics of stressed ($s_{AD}(n)$) and control ($c_{AD}(n)$) animals (Vyas et al., 2002). For instance, to specify the amount of DL to be pruned in shell n on the apical side, we take a sample z of the distribution $\frac{s_{AD}(n)}{c_{AD}(n)}$ (see equation 6.3) and set $\zeta_{AD}(n) = (1 - z)\mathcal{S}_{AD}(n)$. The following algorithm elaborates on this specification procedure:[1]

Algorithm SetSpecifications
Inputs: $\mu^s,\ \mu^c,\ \sigma^s,\ \sigma^c$
Output: ζ

1. Obtain random numbers ζ^s and ζ^c corresponding to the (independent) distributions $N(x; \mu^s, \sigma^s)$ and $N(x; \mu^c, \sigma^c)$, respectively, using the Polar method (Knuth, 1997). Find the ratio $\frac{\zeta^s}{\zeta^c}$.

2. The ratio $\frac{\zeta^s}{\zeta^c}$ is an instance of the random variable,

$$r = \frac{\mu^s + \sigma^s x}{\mu^c + \sigma^c y}, \tag{6.1}$$

where x and y are independent standard normal distributed random variables. Map r to the representation of Marsaglia's ratio distribution (Marsaglia, 1965) as follows:

$$r = k\,\frac{a + x}{b + y}; \qquad k = \frac{\sigma^s}{\sigma^c},\ a = \frac{\mu^s}{\sigma^s},\ b = \frac{\mu^c}{\sigma^c}. \tag{6.2}$$

The probability density function of $\frac{r}{k} = \frac{a+x}{b+y}$ is given as (Marsaglia, 1965)

$$f(t) = \frac{\exp(-0.5(a^2 + b^2))}{\pi(1 + t^2)}\left(1 + \frac{q}{g(q)}\int_o^q g(z)dz\right),$$
$$q = \frac{at + b}{\sqrt{1 + t^2}}, \tag{6.3}$$

where $g(z)$ is the density function of the standard normal deviate. As $\frac{\zeta^s}{\zeta^c}$ is an instance of r, to obtain the corresponding instance of $\frac{r}{k} = \frac{a+x}{b+y}$, scale $\frac{\zeta^s}{\zeta^c}$ by k and set $\widetilde{t}$ as:

$$\widetilde{t} = \frac{1}{k}\,\frac{\zeta^s}{\zeta^c} = \frac{\sigma^c \zeta^s}{\sigma^s \zeta^c}. \tag{6.4}$$

[1] For brevity, a general method to generate ζ, given $\mathcal{S}$, $\mu^s,\ \mu^c\ \sigma^s$, and σ^c, is presented. This holds for all $\zeta_{kl}(n)$ given $\mathcal{S}_{kl}(n)$, $\mu^s_{kl}(n),\ \mu^c_{kl}(n)\ \sigma^s_{kl}(n)$ and $\sigma^c_{kl}(n)$; $k \in \{A, B\},\ l \in \{B, D\},\ n = 0, 1, \ldots, N_k - 1$.

3. Find $f(t = \widetilde{t})$ from equations 6.3 and 6.4.
4. if $(0 \leq f(\widetilde{t}) \leq 1 \ \ \& \ \ f(\widetilde{t}) \geq 0.75 * \max_t(f(t)))$
   accept $\frac{\zeta^s}{\zeta^c}$ as a representative sample of r.
   return $\zeta = \mathcal{S}\left(1 - \frac{\zeta^s}{\zeta^c}\right)$ as the amount to be pruned.
   else goto Step 1.

Step 4 of the above algorithm ensures the following:

- $f(t = \widetilde{t})$ lies within the $[0, 1]$ range, such that there is no negative pruning and there is no specification greater than 100% of actual BP or DL.
- $f(t = \widetilde{t})$ is always greater than 75% of the maximum value of $f(t)$. This is to make sure that the pruning specification approaches the mean distribution of the original data.

The problem of matching DLs arises when the algorithm is applied to neurons obtained from the DSArchive. Experimental data provide pruning statistics for apical DLs up to 400 μm and 300 μm for basal dendrites (cf. Figure 1 of Vyas et al., 2002). However, CA3b pyramidal neurons from the DSArchive have DLs greater than these experimentally reported values. In order to circumvent this problem, statistics for shells with DL less than and equal to these values are set with statistics from Vyas et al. (2002). The statistics of the last shell (shell 8 on the apical side and shell 6 on the basal side) are replicated for shells with DL greater than these values.

7 Specification of Pruning Probabilities

As outlined in Figure 1, once the pruning specifications are set, we need to set probabilities of pruning for DL or BP in any given shell based on the specifications obtained from the SetSpecifications algorithm. Intuitively, if the specification mentions that a given shell has to undergo higher pruning with respect to the other shells, then the probability of pruning for that shell has to be higher. Because the pruning algorithm we employ is an iterative one, within a given shell, we also take into account the current pruning values to specify the probabilities of subsequent pruning.

7.1 DL Pruning Probabilities. These are computed by normalizing the current pruning specifications such that the sum of the probabilities is one. Specifically, the DL pruning probabilities are set as follows:

$$\rho_{kD}(n) = \frac{\zeta_{kD}(n) - \phi_{kD}(n)}{\sum_{k,n}(\zeta_{kD}(n) - \phi_{kD}(n))}, \quad n = 1, \ldots, N_k - 1. \tag{7.1}$$

7.2 BP Pruning Probabilities. Although DL and BP pruning are different numbers in terms of specifications and experimental statistics, they are

physically linked, as they constitute the same dendritic tree. An important goal of our algorithm is to ensure that the reduction schedules of BP and DL remain in synchrony through all the iterations of the algorithm.

Given that for a specific shell n, $\zeta_{kB}(n)$ number of BPs have to be pruned for a $\zeta_{kD}(n)$ reduction in DL, we enforce this by setting the BP pruning probabilities such that, on average, one BP is removed for every $\frac{\zeta_{kD}(n)}{\zeta_{kB}(n)}$ reduction in DL:

$$\rho_{kB}(n) = \rho_{kD}(n)^P \qquad \text{with} \qquad P = \frac{\zeta_{kD}(n)\phi_{kB}(n)}{\zeta_{kB}(n)\phi_{kD}(n)}. \tag{7.2}$$

In order to explain the motivation behind the above equation, we rewrite it as the following set of equations:

$$\widetilde{\rho}_{kB}(n) = \rho_{kD}(n)^{P_1} \qquad \text{with} \qquad P_1 = \frac{\zeta_{kD}(n)}{\zeta_{kB}(n)} \tag{7.3}$$

$$\rho_{kB}(n) = \widetilde{\rho}_{kB}(n)^{P_2} \qquad \text{with} \qquad P_2 = \frac{\phi_{kB}(n)}{\phi_{kD}(n)}. \tag{7.4}$$

The expression for $\widetilde{\rho}_{kB}(n)$, equation 7.3, states that for one BP to be pruned, as per the specifications, on average, P_1 units of DL are required to be pruned. Equation 7.4 modulates this base expression with current pruning values $\phi_{kl}(n)$, ensuring that BP pruning runs according to schedule with respect to DL pruning.

It may be noted here that the value of P in equation 7.2 determines whether BP pruning is on par or not with respect to DL pruning. This can be easily confirmed if P is seen as the ratio of P_1 and $\frac{1}{P_2}$. If $P > 1$, then BP pruning is ahead of schedule; in this case, $\rho_{kB}(n)$ is set to be less than $\rho_{kD}(n)$ as per equation 7.2, which means that the probability of pruning a BP has been decreased with respect to that of pruning a DL, thus forcing BP pruning to slow down. Similarly, if $P > 1$, BP pruning would be running behind schedule and $\rho_{kB}(n) > \rho_{kD}(n)$, meaning that BP pruning becomes more probable than DL pruning. Finally, BP pruning is on schedule with respect to DL pruning if $P = 1$. Effectively, P, which gets updated at each iteration of the algorithm (being dependent on $\phi_{kl}(n)$), ensures the requirement that, on average, one BP is removed for every $\frac{\zeta_{kD}(n)}{\zeta_{kB}(n)}$ reduction in DL.

8 Pruning the Dendritic Tree

Our pruning algorithm is an iterative process that selects a given shell in each iteration, based on the pruning probabilities derived above, and prunes either 1 μm of DL or one BP. An adaptation of the rejection method for generating random numbers (Knuth, 1997) is employed to select the shells within which pruning of DL and BP is to be executed. Similar methods have been used in models of dendritic growth and for pruning simple, virtual dendritic trees (van Pelt, Dityatev, & Uylings, 1997; van Pelt, 1997).

The steps involved in pruning DL (in steps of 1 μm) or a BP, as part of a single iteration, are:

1. Select a BP or a terminal dendritic point randomly using a uniformly distributed random number generator.
2. Find the shell number $\widetilde{n}$ to which the point belongs.
3. Generate a random number *rand* from a uniform distribution.
4. DL pruning: If ($rand < \rho_{kD}(\widetilde{n})$), prune 1 μm length starting from the terminal point, reduce $\phi_{kD}(\widetilde{n})$ by unit value, and update $\rho_{kD}(\widetilde{n})$ and $\rho_{kB}(\widetilde{n})$ as in equations 7.1 and 7.2, respectively.
5. BP pruning: If ($rand < \rho_{kB}(\widetilde{n}) \prod_{m\in\mathcal{S}} \rho_{kD}(m)^{R_m}$), prune the dendrite that connects the BP to a terminal point, reduce $\phi_{kB}(\widetilde{n})$ by one, and update $\phi_{kD}(\widetilde{n})$. Modify $\rho_{kD}(\widetilde{n})$ and $\rho_{kB}(\widetilde{n})$ as in equations 7.1 and 7.2, respectively.

The algorithm converges when $\max_{k,l,n} \frac{\zeta_{kl}(n)-\phi_{kl}(n)}{\zeta_{kl}(n)} < T$ (with a default value of $T = 0.001$), where T gives the allowance threshold for the maximum error in specifications. If the algorithm does not converge satisfactorily in certain shells due to the organization of the dendrites in some trees, post-processing is done on those shells alone to make sure that the pruned tree meets the specifications.

In the above scheme, we use the fact that a BP ceases to exist if one of the two subtrees originating from it is completely removed. We remove a BP by removing all the dendritic points present between it and its corresponding terminal point (with no other BP in between). For instance, if the BP represented by BP_t in Figure 3 is to be pruned, one has to remove either DL_{tt1} or DL_{tt2}, so that BP_t ceases to be a BP. This removal of dendritic length should also be taken into account in setting the probability of pruning a BP. This is done by revising the probability for pruning the BP as (step 5 above):

$$\rho'_{kB}(\widetilde{n}) = \rho_{kB}(\widetilde{n}) \prod_{m\in\mathcal{P}} \rho_{kD}(m)^{R_m}, \tag{8.1}$$

where $\rho_{kB}(\widetilde{n})$ is as in equation 7.2. The set $\{R_m : m \in \mathcal{P}\}$ refers to the dendritic points that are present between the pruned BP and the corresponding terminal point, where $\mathcal{P}$ corresponds to the set of all the Sholl shells through which these sets of points traverse. With reference to the illustration in Figure 3, if DL_{tt1} is chosen for pruning, then $\mathcal{P} = \{3, 4, 5\}$ as DL_{tt1} traverses through shells 3, 4, and 5 (see Figure 3).

Pruning a nonterminal branch point involves more constraints than pruning a terminal branch point. The difference between pruning a terminal and nonterminal branches is depicted in Figure 3. The probability of pruning the terminal branch BP_t is a product of the probability of pruning BP_t alone and pruning DL_{tt1} through $\mathcal{P}$, as given by equation 8.1. On the other hand,

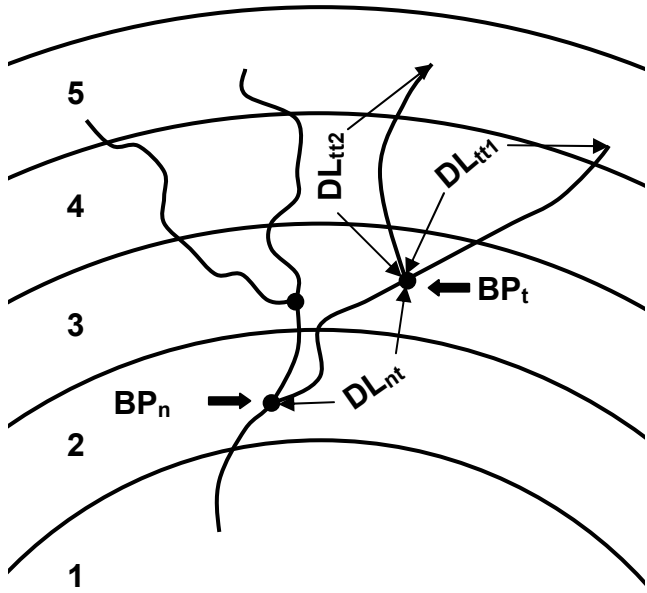

Figure 3: Illustration of pruning terminal and nonterminal BPs. Dendritic subtree overlaid on concentric shells, used in Sholl's analysis, indicating typical terminal (BP_t) and nonterminal (BP_n) BPs. DL_{nt} corresponds to the DL between BP_n and BP_t. DL_{tt1} and DL_{tt2} represent DLs between BP_t and its terminal points. The numerical indices on the left correspond to the shell numbers.

the probability of pruning the nonterminal branching point BP_n would be a product of the probabilities of pruning BP_n alone, pruning DL_{nt}, pruning BP_t, and pruning DL_{tt1} and DL_{tt2}. This product turns out to have a very low value for all nonterminal branch points, and omitting these did not cause any difference in the pruning procedure. Hence we do not consider nonterminal branching points for pruning unless they eventually become terminal branches during the pruning process.

9 Results

A Linux system running on a Pentium IV processor is used for all computations. The pruning algorithm is implemented in C++. A typical execution of the algorithm takes less than 1 minute for a CA3b pyramidal cell from the DSArchive. The total DL of typical CA3 pyramidal neurons is in the range of 1.2 mm to 1.5 mm, with the apical tree covering around 0.7 mm of the total length (approximately 60–65% of the total DL). The total number of BPs is around 60 to 75 in these neurons.

In order to test the algorithm, we generate 100 sets of specifications using the SetSpecifications algorithm, and run the pruning algorithm with these specifications. We then perform Sholl's analysis on these pruned neurons and plot their statistics (see Figure 4). Figure 4A illustrates, as a function of the radial distance from the soma, the region-specific reduction in DL of the pruned neurons (equivalent to an experimental neuron that has undergone stress-induced atrophy) with respect to the original neuron (equivalent to a control unstressed neuron). Figure 4B displays the effects on the number of BPs.

Several features of the results depicted in Figure 4 are particularly relevant with respect to experimental data on stress-induced dendritic atrophy. First, the most significant pruning is evident at a distance of 100 to 300 μm from the soma on apical dendrites, that is, in the stratum radiatum of area CA3. This is in agreement with experimental observations in several studies (Vyas et al., 2002; McEwen, 1999; Watanabe et al., 1992).

Second, we carried out a more quantitative analysis to further validate this qualitative agreement between experimental data and results obtained from our pruning algorithm (see Figure 5). As described in section 6, the algorithm is designed to emulate the ratio of pruning BP and DL along all dendritic shells. Thus, we compare the modes of the reduction distribution[2] obtained from experimental data and from the outcomes of our algorithm for each shell along the apical and basal sides.

The methods used to compute the experimental and algorithmic modes of the reduction distribution are explained in Figure 5A. This illustration employs the dendritic length of a shell located at 400 μm from the soma on the apical side as an example. We use biological atrophy data (Vyas et al., 2002) and equation 6.3 to generate the distribution of percentage reductions in the dendritic length. The percentage value at which this distribution attains its maximum corresponds to the experimental mode of the distribution (see Figure 5A, left). The distributions that are used for computing these modes are $1 - \frac{s_{kl}(n)}{c_{kl}(n)}$ $n = 0, 1, \ldots, N_k - 1,\ k \in \{A, B\},\ l \in \{B, D\}$, and for the given example, it is $1 - \frac{s_{AD}(8)}{c_{AD}(8)}$.

We then determine the algorithm modes by following these steps (see Figure 5A, right): (1) generate 100,000 different specifications on a given model neuron, (2) prune the given neuron exactly to these specifications using the algorithm, (3) obtain Sholl's analysis for each of the 100,000 outcomes, (4) plot the histograms of each of $\mathcal{S}_{kl}(n)$ for $n = 0, 1, \ldots, N_k - 1,\ k \in \{A, B\},\ l \in \{B, D\}$ (i.e., the output of Sholl's analysis) using all the 100,000 outcomes, and (5) compute the mode of the histograms. Figure 5A also

[2] $\frac{s_{kl}(n)}{c_{kl}(n)}$ corresponds to the ratio distribution of statistics from the stressed and control animals. Reduction distribution corresponds to the distribution of reduction in DL/BP in stressed neurons with respect to control neurons and is represented as $1 - \frac{s_{kl}(n)}{c_{kl}(n)}$.

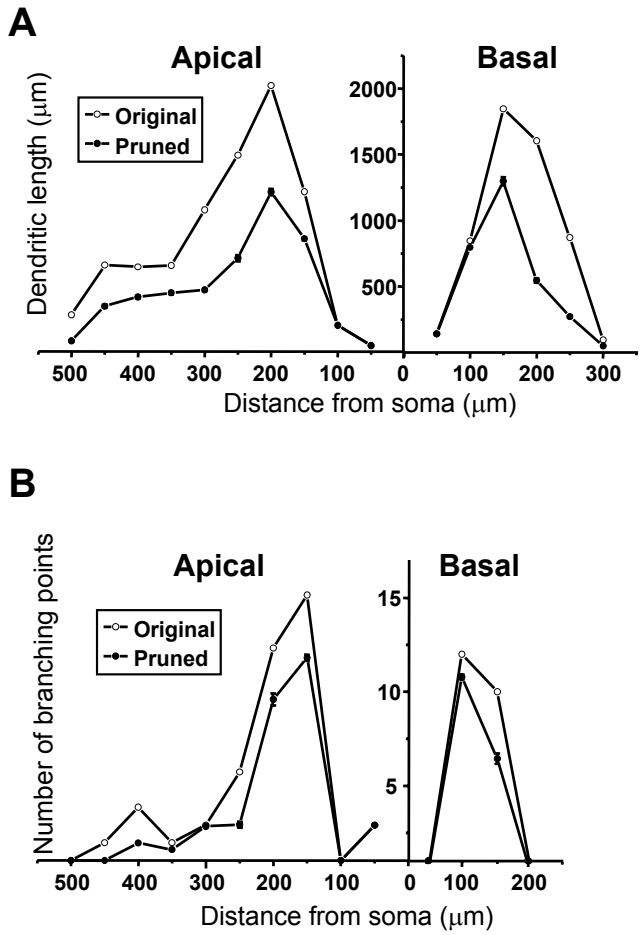

Figure 4: Pruning algorithm replicates experimental dendritic atrophy in 3D reconstructions of CA3 pyramidal cells. (A) Dendritic length (μm) as a function of the radial distance from the soma (μm). Open circles: Shell-wise DL for unpruned neuron; filled circles: mean and SEM of shell-wise DL of 100 neurons pruned with specifications set in the range of changes experimentally observed following chronic stress. (B) Branching points as a function of the radial distance from the soma (μm). Open circles: Shell-wise count of BPs on apical and basal sides for unpruned neuron; Filled circles: mean and SEM of shell-wise BPs of 100 neurons used in *A*.

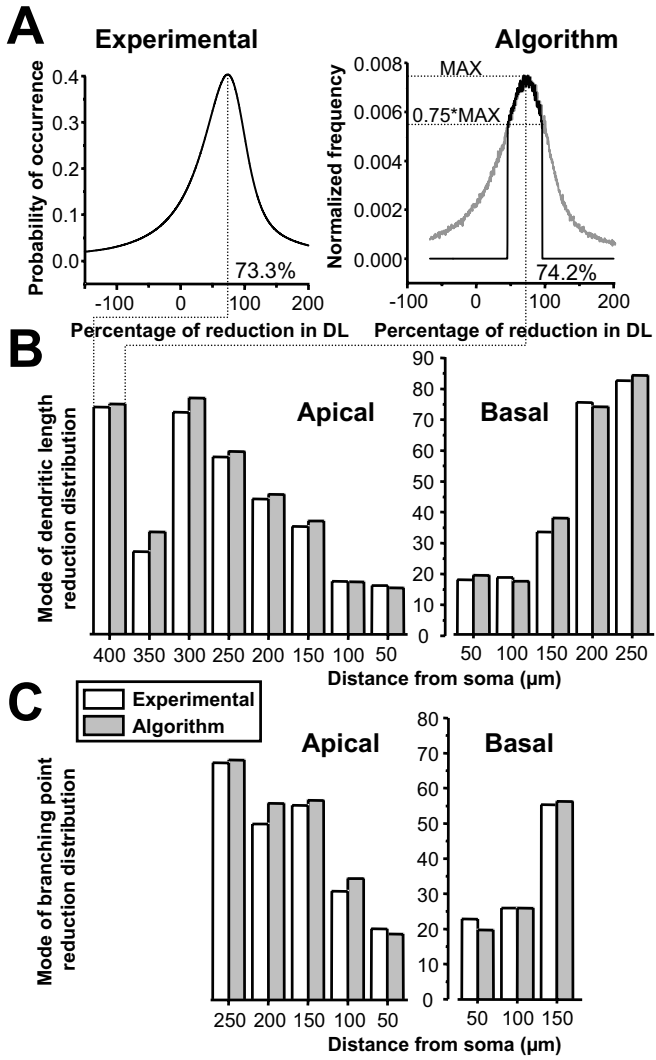

brings out the accuracy of the pruning procedure by showing that within the valid specification range (indicated by the solid vertical lines, Figure 5A, right), there is complete overlap between the pruning specifications (gray curve) and the outcomes of the algorithm (black curve).

Using the process depicted in Figure 5A, modes of percentage reduction distribution for DL (see Figure 5B) and BP (see Figure 5C) are plotted for each shell as a function of its distance from the soma. As Figures 5B and 5C depict, this analysis confirmed that the modes of the reduction distributions

obtained from biological data (see Figures 5B and 5C, "experimental," open bars) match the outcomes of our pruning algorithm (see Figures 5B and 5C, "algorithm," gray bars) in all dendritic regions. The maximum discrepancy is found to be less than 5% in all comparisons involving the modes of DL and BP reduction along all shells on the apical and basal sides.

Finally, a further point of agreement between our results and experimental data is with reference to the reduction in total dendritic length. Stress-induced atrophy in total dendritic length has been reported to be at around 30% in CA3 pyramidal cells (Watanabe et al., 1992; Vyas et al., 2002). This is in agreement with the outcome of our algorithm, which prunes 30% to 45% of the total dendritic length, while maintaining region specificity in the process (see Figure 6). It may also be observed from Figure 6 that the stratum radiatum (the region between the two dotted lines) has undergone maximal pruning relative to the other regions of the neuron, which is also consistent with the experimentally obtained data on stress-induced dendritic atrophy (Watanabe et al., 1992; Vyas et al., 2002).

While the pruning algorithm is capable of eliciting specific patterns of dendritic remodeling that match experimental observations rather well, it should also be noted that our algorithm can prune a given tree to various degrees of atrophy under a specified probabilistic regime (see Figure 6). This helps in obtaining trees of any desired level of atrophy with the relative reductions in BP and DL across various shells maintained as per the specifications. This feature is a direct outcome of the iterative nature of the

Figure 5: *Facing page*. Agreement between shell-specific modes of percentage reduction distributions observed biologically and calculated from the algorithmic outcomes. (A) Illustration of the calculation of modes of the reduction distribution for DL, using the example of a shell located at 400 μm from the soma on the apical side. Experimental mode (left) is computed by finding the point at which the reduction distribution (obtained from equation 6.3) attains its maximum value. The mode of reduction distribution corresponding to the algorithm (right) is obtained by finding the histogram of Sholl's analysis outcomes of the pruned neurons (curve highlighted in black). The plot in gray depicts the samples of the reduction distribution that were used to arrive at the pruning specifications. The 0.75*MAX value (dotted horizontal line) indicates the constraint imposed by the SetSpecifications algorithm (step 4) to determine the samples that are considered valid specifications. This, along with the other constraint that the sample has to lie between 0 and 100% (step 4 of the SetSpecifications algorithm), constitutes the difference between the gray and black curves. Within the valid specification range (indicated by the solid vertical lines), there is complete overlap between the pruning specifications (gray curve) and the outcomes of the algorithm (black curve). Using the process depicted in *A*, modes of reduction distribution for DL (B) and BP (C) are computed for each shell as a function of distance from the soma.

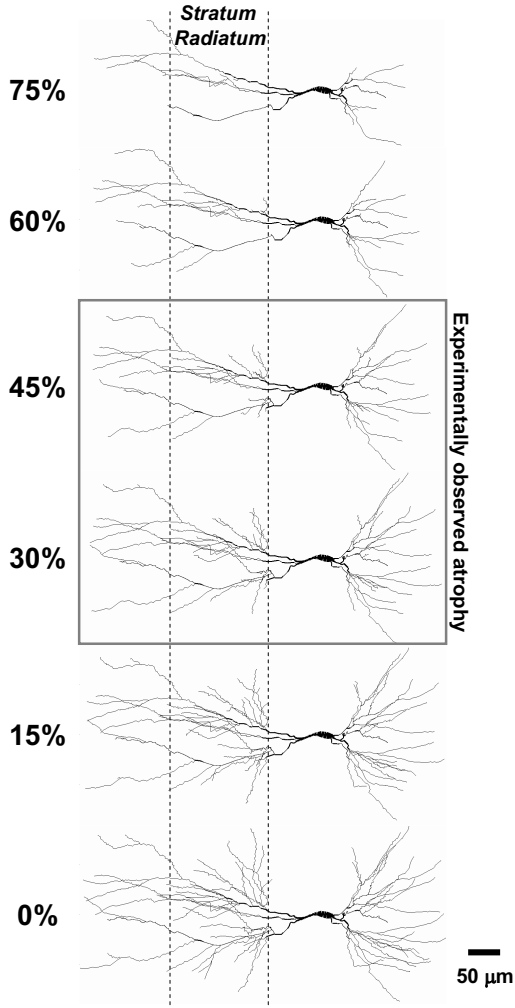

Figure 6: A wide range of dendritic atrophy can be achieved using the pruning algorithm. Projections of 3D reconstructions of a CA3 pyramidal cell and its various pruned versions. The percentage of pruning is given to the left of each projection. Pruning in the range of 30% to 45% reduction (reconstructions within the gray box) corresponds to the outcomes of the algorithm with specifications set in the range of atrophy observed experimentally after chronic stress in animal models (Vyas et al., 2002; Watanabe et al., 1992). The stratum radiatum (delineated by parallel dotted lines) undergoes maximal dendritic pruning and debranching, which is consistent with experimental data (Vyas et al., 2002; Watanabe et al., 1992).

algorithm, which can be stopped at any given iteration to obtain the tree of desired length. The relative reduction across shells is kept constant because the choice to prune a DL or BP is guided by the probabilistic regime through all the iterations.

10 Discussion

In this study, we have employed chronic stress-induced dendritic atrophy in the hippocampus as a model to develop an algorithm to elicit systematic, region-specific remodeling of 3D reconstructions of CA3 pyramidal neurons. While it is standard practice to find the ratio of the means of two distributions to determine the amount of reduction, in our model, we have employed the actual ratio distribution to arrive at the statistics of the ratio. Using this ratio distribution, we have calculated region-based distributions of reduction in dendritic arborization, which are used to characterize the region-specific pruning probabilities at any given distance from the soma. These probabilities then drive an iterative algorithm, which probabilistically reduces either 1 μm of dendritic length or removes one branching point in each iteration. There are two distinct advantages of this algorithm. First, it prunes BP and DL in parallel, both within the same probabilistic framework, thus ensuring that the average pruning in DL per BP is maintained through all iterations (see equation 7.2). Second, it provides precise control over the remodeling process at any point of interest with the relative pruning across various regions still conforming to biological data. This helps in analyzing the causal structure-function relationship over a range of remodeling by maintaining region specificity throughout, thereby allowing us to monitor the evolution of the neuron's biological function as the remodeling proceeds.

It is also important to emphasize that although we used stress-induced dendritic atrophy as a test case, the algorithm presented here is a generalized one that can be applied to a wide range of biological problems involving dendritic remodeling. In other words, this algorithm can be applied to induce both growth and pruning of neuronal reconstructions. In problems involving dendritic growth, the only difference would be to add a BP or 1 μm of DL once a specific region is probabilistically selected. Further, for simulating dendritic growth, the diameter of the newly formed dendrites should also be fixed, which can be done using Rall's branching rule (Rall, 1977).

A related class of algorithms for generating virtual dendritic trees to match a given statistical framework is the L-Neuron package (Ascoli & Krichmar, 2000; Ascoli, Krichmar, Scorcioni, Nasuto, & Senft, 2001). Our algorithm is different from these because here we remodel real 3D reconstructions based on experimental data, whereas L-Neuron generates virtual neurons based on morphometric data. Further, for analyzing the effects of localized remodeling, our algorithm has the advantage of generating neu-

rons for possible analysis of causal structure-function relationships. This is possible because we remodel dendrites of a given neuron to various levels of atrophy, and the extent and location of the reduction are well known. This is in contrast to, say, having two groups of neurons generated to match the stress and control statistics and using them for analyzing the structure-function relationship. Such an analysis can provide us with only correlative relationships rather than precise causal relationships, as the analysis is not confined to remodeling a given neuron.

Given that systematic manipulation of dendritic morphology is currently impossible with biological neurons, the framework presented here provides us with a tool to quantitatively address questions related to specific contributions of dendritic structure to neuronal function during both neuronal development and experience-induced plasticity in adults. The region specificity of the outputs of the algorithm opens new avenues to address the exciting possibility that localized changes in dendritic structure translate to localized changes in neuronal function. It also allows us to analyze the effects of possible local modulation of ionic and synaptic channels as a result of dendritic remodeling. Such analysis may have significant implications for recent findings related to intrinsic plasticity in neurons (Frick et al., 2004).

Acknowledgments

This work was supported by a research grant from the Department of Biotechnology, India. We express grateful thanks to Ajai Vyas and Rupshi Mitra for helpful discussions. We also thank the anonymous reviewer for the positive comments and suggestions, which helped substantially in improving the presentation of this article.

References

Anderton, B. H., Callahan, L., Coleman, P., Davies, P., Flood, D., Jicha, G. A., Ohm, T., & Weaver, C. (1998). Dendritic changes in Alzheimer's disease and factors that may underlie these changes. *Progress in Neurobiology, 55*, 595–609.

Ascoli, G., & Krichmar, J. L. (2000). L-Neuron: A modeling tool for the efficient generation and parsimonious description of dendritic morphology. *Neurocomputing, 32–33*, 1003–1011.

Ascoli, G., Krichmar, J., Scorcioni, R., Nasuto, S., & Senft, S. (2001). Computer generation and quantitative morphometric analysis of virtual neurons. *Anatomy and Embryology, 204*, 283–301.

Berzhanskaya, J., Urban, N. N., & Barrionuevo, G. (1998). Electrophysiological and pharmacological characterization of the direct perforant path input to hippocampal area CA3. *Journal of Neurophysiology, 79*, 2111–2118.

Bothwell, S., Meredith, G. E., Phillips, J., Staunton, H., Doherty, C., Grigorenko, E., Glazier, S., Deadwyler, S., O'Donovan, C. A., & Farrell, M. (2001). Neuronal hypertrophy in the neocortex of patients with temporal lobe epilepsy. *Journal of Neuroscience, 21*, 4789–4800.

Brizzee, K. R. (1987). Neurons numbers and dendritic extent in normal aging and Alzheimer's disease. *Neurobiology of Aging, 8*, 579–580.

Cannon, R., Turner, D., Pyapali, G., & Wheal, H. (1998). An on-line archive of reconstructed hippocampal neurons. *Journal of Neuroscience Methods, 84*, 49–54.

Cline, H. T. (2001). Dendritic arbor development and synaptogenesis. *Current Opinion in Neurobiology, 11*, 118–126.

Cossart, R., Epsztein, J., Tyzio, R., Becq, H., Hirsch, J., Ben-Ari, Y., & Crepel, V. (2002). Quantal release of glutamate generates pure kainate and mixed AMPA/kainate EPSCs in hippocampal neurons. *Neuron, 35*(1), 147–159.

Duan, H., Wearne, S. L., Rocher, A. B., Macedo, A., Morrison, J. H., & Hof, P. R. (2003). Age-related dendritic and spine changes in corticocortically projecting neurons in macaque monkeys. *Cerebral Cortex, 13*, 950–961.

Frick, A., Magee, J., & Johnston, D. (2004). LTP is accompanied by an enhanced local excitability of pyramidal neuron dendrites. *Nature Neuroscience, 7*, 126–135.

Geula, C. (1998). Abnormalities of neural circuitry in Alzheimer's disease: Hippocampus and cortical cholinergic innervation. *Neurology, 51*, S18–S29.

Häusser, M., & Mel, B. (2003). Dendrites: Bug or feature? *Current Opinion in Neurobiology, 13*, 372–383.

Johnston, D., & Amaral, D. G. (1997). Hippocampus. In G. Shepherd (Ed.), *Synaptic organization of the brain* (4th ed.). New York: Oxford University Press.

Johnston, D., Magee, J. C., Colbert, C. M., & Cristie, B. R. (1996). Active properties of neuronal dendrites. *Annual Review of Neuroscience, 19*, 165–186.

Jones, T. A., & Schallert, T. (1994). Use-dependent growth of pyramidal neurons after neocortical damage. *Journal of Neuroscience, 14*, 2140–2152.

Kaufmann, W. E., & Moser, H. W. (2000). Dendritic anomalies in disorders associated with mental retardation. *Cerebral Cortex, 10*, 981–991.

Keyvani, K., & Schallert, T. (2002). Plasticity-associated molecular and structural events in the injured brain. *Journal of Neuropathology and Experimental Neurology, 61*, 831–840.

Knuth, D. E. (1997). *The art of computer programming, Vol. 2: Seminumerical algorithms* (3rd ed.). Reading, MA: Addison-Wesley.

Krichmar, J. L., Nasuto, S. J., Scorcioni, R., Washington, S. D., & Ascoli, G. A. (2002). Effects of dendritic morphology on CA3 pyramidal cell electrophysiology: A simulation study. *Brain Research, 941*, 11–28.

Magee, J., Hoffman, D., Colbert, C., & Johnston, D. (1998). Electrical and calcium signaling in dendrites of hippocampal pyramidal neurons. *Annual Review of Physiology, 60*, 327–346.

Mainen, Z., & Sejnowski, T. (1996). Influence of dendritic structure on firing pattern in model neocortical neurons. *Nature, 382*, 363–366.

Marc, R. E., Jones, B. W., Watt, C. B., & Strettoi, E. (2003). Neural remodeling in retinal degeneration. *Progress in Retinal and Eye Research, 22*, 607–655.

Marsaglia, G. (1965). Ratios of normal variables and ratios of sums of uniform variables. *American Statistical Association Journal, 60*, 193–204.

McEwen, B. (1999). Stress and hippocampal plasticity. *Annual Review of Neuroscience, 22*, 105–122.

Migliore, M., & Shepherd, G. M. (2002). Emerging rules for the distributions of active dendritic conductances. *Nature Reviews Neuroscience, 3*, 362–370.

Popov, V. I., Bocharova, L. S., & Bragin, A. G. (1992). Repeated changes of dendritic morphology in the hippocampus of ground squirrels in the course of hibernation. *Neuroscience, 48*, 45–51.

Pyapali, G. K., & Turner, D. A. (1996). Increased dendritic extent in hippocampal CA1 neurons from aged F344 rats. *Neurobiology of Aging, 17*, 601–611.

Rall, W. (1977). Core conductor theory and cable properties of neurons. In E. R. Kandel (Ed.), *Handbook of physiology* (Sec. 1, Vol. 1, pp. 39–97). Bethesda, MD: American Physiological Society.

Ramakers, G. J. (2002). Rho proteins, mental retardation and the cellular basis of cognition. *Trends in Neuroscience, 25*, 191–199.

Regehr, W. G., & Tank, D. W. (1994). Dendritic calcium dynamics. *Current Opinion in Neurobiology, 4*, 373–382.

Segev, I., & London, M. (2000). Untangling dendrites with quantitative models. *Science, 290*, 744–750.

Sholl, D. A. (1953). Dendritic organization in the neurons of the visual and motor cortices of the cat. *Journal of Anatomy, 87*, 387–406.

Stuart, G., Spruston, N., & Häusser, M. (Eds.). (1999). *Dendrites*. New York: Oxford University Press.

Traub, R. D., Jefferys, J. G. R., & Whittington, M. A. (1999). *Fast oscillations in cortical circuits*. Cambridge, MA: MIT Press.

van Ooyen, A., Duijnhouwer, J., Remme, M. W., & van Pelt, J. (2002). The effect of dendritic topology on firing patterns in model neurons. *Network: Computation in Neural Systems, 13*, 311–325.

van Ooyen, A., Willshaw, D. J., & Ramakers, G. J. A. (2000). Influence of dendritic morphology on axonal competition. *Neurocomputing, 32–33*, 255–260.

van Pelt, J. (1997). Effect of pruning on dendritic tree topology. *Journal of Theoretical Biology, 186*, 17–32.

van Pelt, J., Dityatev, A. E., & Uylings, H. B. M. (1997). Natural variability in the number of dendritic segments: Model-based inferences about branching during neurite outgrowth. *Journal of Comparative Neurology, 387*, 325–340.

Vetter, P., Roth, A., & Häusser, M. (2001). Propagation of action potentials in dendrites depends on dendritic morphology. *Journal of Neurophysiology, 85*, 926–937.

Vyas, A., Mitra, R., Rao, B. S. S., & Chattarji, S. (2002). Chronic stress induces contrasting patterns of dendritic remodeling in hippocampal and amygdaloid neurons. *Journal of Neuroscience, 22*, 6810–6818.

Wang, Z., Xu, N. L., Wu, C. P., Duan, S., & Poo, M. M. (2003). Bidirectional changes in spatial dendritic integration accompanying long-term synaptic modifications. *Neuron, 37*, 463–472.

Watanabe, Y., Gould, E., & McEwen, B. S. (1992). Stress induces atrophy of apical dendrites of hippocampal CA3 pyramidal neurons. *Brain Research, 588*(2), 341–345.

Wong, R. O. L., & Ghosh, A. (2002). Activity-dependent regulation of dendritic growth and patterning. *Nature Reviews Neuroscience, 3*, 803–812.

Received February 3, 2004; accepted June 2, 2004.